

Spin, charge and orbital fluctuations in a multi-orbital Mott insulator

Akihisa Koga and Norio Kawakami

Department of Applied Physics, Osaka University, Suita, Osaka 565-0871, Japan

T.M. Rice and Manfred Sigrist

Theoretische Physik, ETH-Hönggerberg, 8093 Zürich, Switzerland

(Dated: November 11, 2018)

The two-orbital degenerate Hubbard model with distinct hopping integrals is studied by combining dynamical mean-field theory with quantum Monte Carlo simulations. The role of orbital fluctuations for the nature of the Mott transition is elucidated by examining the temperature dependence of spin, charge and orbital susceptibilities as well as the one-particle spectral function. We also consider the effect of the hybridization between the two orbitals, which is important particularly close to the Mott transition points. The introduction of the hybridization induces orbital fluctuations, resulting in the formation of a Kondo-like heavy-fermion behavior, similarly to f electron systems, but involving electrons in bands of comparable width.

PACS numbers: 71.10.Fd, 71.30.+h

I. INTRODUCTION

Strongly correlated electron systems with multi-orbital bands pose a variety of intriguing problems. One of the recently debated topics is the orbital-selective Mott transition (OSMT) in highly correlated d -electron systems.^{1,2,3,4,5,6} It is a fundamental issue of multi-orbital systems whether Mott-transitions would take place in sequence or simultaneously for all bands, if correlation would gradually be turned on. There are however also specific materials which have been discussed in this context such as the calcium-doped single layer strontium ruthenate $\text{Ca}_{2-x}\text{Sr}_x\text{RuO}_4$ ⁷ and the ternary nickel oxide $\text{La}_{n+1}\text{Ni}_n\text{O}_{3n+1}$,^{8,9} where the chemical substitution (or the change in the temperature) may trigger the OSMT in the t_{2g} (e_g) orbitals in the former (latter) case.

The extensive studies on the Mott transition in the multi-orbital systems clarified that the competition between the intra- and inter-orbital interactions as well as the Hund coupling plays a key role to determine the nature of the Mott transition.³ It was found that under special conditions in a two-band system the Mott-transitions may merge to a single one, but would split for a generic form of the model. In particular, the presence of Hund coupling seems to be essential to observe distinct transitions. These conclusions were drawn from the analysis of the quasi-particle weights computed at zero temperature. In order to characterize the transitions the behavior of the spin, charge and orbital fluctuations provides additional valuable information. A systematic study of the temperature dependence of certain susceptibilities will give us the necessary insight to analyze in particular the electronic degrees of freedom which are localized through the Mott transition.

The above discussions on the Mott transition are restricted so far to systems for which the bands do not hybridize, but are coupled to each other only through electron-electron interactions. However, the hybridization between the bands may be important in some

compounds.¹⁰ In particular, this effect could give rise to a qualitative change in the phase diagram, when there occurs the OSMT, for which the intermediate phase appears with one orbital localized and the other itinerant. One thus naively wonders whether Kondo-like heavy fermion states would be induced by the hybridization between the orbitals. In fact, certain observed features can possibly be attributed to Kondo like behavior in the compound $\text{Ca}_{2-x}\text{Sr}_x\text{RuO}_4$ ($0.2 < x < 0.5$),⁷ where the hybridization between orbitals is induced by the tilting of RuO_6 octahedra.¹¹ It is surprising that this behavior emerges from electrons which originate from bands of comparable width. These interesting observations naturally motivate us to explore the effect of hybridization in more detail.

In this paper, we study a two-orbital Hubbard model with the distinct hopping integrals by combining dynamical mean field theory (DMFT)^{12,13,14,15} with quantum Monte Carlo (QMC) simulations.^{16,17} We examine the spin, charge and orbital fluctuations which give insight into the electronic properties in the regime of the OSMT. We further consider the effect of hybridization, which may be important in real materials, and show that heavy-fermion-like behavior emerges upon introduction of the hybridization. The paper is organized as follows. In §II, we introduce the model Hamiltonian for the two-orbital system and briefly explain the framework of DMFT. We discuss how the spin and orbital fluctuations affect the metal-insulator transition in §III. A brief summary is given in the last section.

II. MODEL AND METHOD

We consider the following two-orbital Hubbard Hamiltonian,

$$H = \sum_{\substack{\langle i,j \rangle \\ \alpha\beta\sigma}} t_{ij}^{(\alpha\beta)} c_{i\alpha\sigma}^\dagger c_{j\beta\sigma} + U \sum_{i\alpha} n_{i\alpha\uparrow} n_{i\alpha\downarrow}$$

$$\begin{aligned}
& + (U' - J) \sum_{i\sigma} n_{i1\sigma} n_{i2\sigma} + U' \sum_{i\sigma} n_{i1\sigma} n_{i2\bar{\sigma}} \\
& - J \sum_i \left[c_{i1\uparrow}^\dagger c_{i1\downarrow} c_{i2\downarrow}^\dagger c_{i2\uparrow} + c_{i1\downarrow}^\dagger c_{i1\uparrow} c_{i2\uparrow}^\dagger c_{i2\downarrow} \right] \\
& - J \sum_i \left[c_{i1\uparrow}^\dagger c_{i1\downarrow}^\dagger c_{i2\uparrow} c_{i2\downarrow} + c_{i2\uparrow}^\dagger c_{i2\downarrow}^\dagger c_{i1\uparrow} c_{i1\downarrow} \right] \quad (1)
\end{aligned}$$

where $c_{i\alpha\sigma}^\dagger (c_{i\alpha\sigma})$ creates (annihilates) an electron with spin $\sigma (= \uparrow, \downarrow)$ and orbital index $\alpha (= 1, 2)$ at the i th site and $n_{i\alpha\sigma} = c_{i\alpha\sigma}^\dagger c_{i\alpha\sigma}$. U (U') represents the intraband (interband) Coulomb interaction and J the Hund coupling. For electron hopping, we introduce

$$t_{ij}^{(\alpha\beta)} = t_{ij}^{(\alpha)} \delta_{\alpha\beta} + V \delta_{ij}, \quad (2)$$

with the orbital-dependent nearest-neighbor hopping $t_{ij}^{(\alpha)}$ and the hybridization V between two orbitals. By this generalized model, we can study several different models in the same framework. For $V = 0$, the system is reduced to the multi-orbital Hubbard model with the same ($t_{ij}^{(\alpha)} = t_{ij}$) or distinct orbitals.^{3,4} On the other hand, for $t_{ij}^{(2)} = 0$, the system is reduced to a correlated electron system coupled to localized electrons, such as the periodic Anderson model ($J = 0$) for heavy-fermion systems^{18,19,20,21,22} or the double exchange model ($J > 0$) for some transition metal oxides.^{23,24,25,26} For general choices of the parameters, we expect a variety of characteristic properties inherent in these limiting models to appear naturally.

To investigate the above degenerate Hubbard model, we make use of DMFT,^{12,13,14,15} which has successfully been applied to various electron systems such as the single band Hubbard model,^{27,28,29,30,31,32,33,34} the multi-orbital Hubbard model,^{3,4,6,17,35,36,37,38,39,40} the periodic Anderson model.^{41,42,43,44,45,46} In DMFT, the lattice model is mapped to an effective impurity model, where local electron correlations are taken into account precisely. The lattice Green function is then obtained via self-consistent conditions imposed on the impurity problem.

In DMFT for the multi-orbital model, the Green function in the lattice system is given as,

$$\mathbf{G}(k, z)^{-1} = \mathbf{G}_0(k, z)^{-1} - \Sigma(z), \quad (3)$$

with

$$\mathbf{G}_0(k, z)^{-1} = \begin{pmatrix} z + \mu - \epsilon_1(k) & -V \\ -V & z + \mu - \epsilon_2(k) \end{pmatrix}, \quad (4)$$

and

$$\Sigma(z) = \begin{pmatrix} \Sigma_{11}(z) & \Sigma_{12}(z) \\ \Sigma_{21}(z) & \Sigma_{22}(z) \end{pmatrix}, \quad (5)$$

where μ is the chemical potential, and $\epsilon_\alpha(k)$ is the bare dispersion relation for the α -th orbital. In terms of the

density of states $\rho(x)$ rescaled by the band width D_α , the local Green function is expressed as,

$$\begin{aligned}
G_{11}(z) &= \int dx \frac{\rho(x)}{\xi_1(z, x) - \frac{v(z)^2}{\xi_2(z, x)}}, \\
G_{12}(z) &= \int dx \frac{v(z)}{\xi_1(z, x) \xi_2(z, x) - v(z)^2}, \\
G_{22}(z) &= \int dx \frac{\rho(x)}{\xi_2(z, x) - \frac{v(z)^2}{\xi_1(z, x)}}, \quad (6)
\end{aligned}$$

where

$$\begin{aligned}
\xi_1(z, x) &= z + \mu - \Sigma_{11} - D_1 x, \\
\xi_2(z, x) &= z + \mu - \Sigma_{22} - D_2 x, \\
v(z) &= V + \Sigma_{12}(z). \quad (7)
\end{aligned}$$

In the following, we use the semicircular density of states $\rho(x) = 2/\pi\sqrt{1-x^2}$.

There are various numerical methods to solve the effective impurity problem. Note that the explicit model Hamiltonian for the impurity system is not obtained straightforwardly in our case, since the lattice Green function has a frequency-dependent term in the non-diagonal element when the system has the hybridization V and the finite band width in both orbitals. Therefore, it is not necessarily most efficient to apply the exact diagonalization²⁷ or the two-site DMFT²⁸ methods as impurity solvers, because these methods require the knowledge of the explicit form of the Hamiltonian. Furthermore, self-consistent perturbation theories such as the iterative perturbation method and the non-crossing approximation are not appropriate to discuss orbital fluctuations in the vicinity of the critical point. In the present study, we make use of QMC to treat the impurity model at finite temperatures.¹⁶ In this connection, we note here that the Hund coupling plays a key role in controlling the nature of the Mott transition in the multi-orbital system.⁶ Therefore, it is important to carefully analyze the effect of the Hund coupling in the framework of QMC. To this end, we use the algorithm proposed by Sakai et al.,¹⁷ where the Hund coupling is represented in terms of discrete auxiliary fields. When we solve the effective impurity model by means of QMC method, we use the Trotter time slices $\Delta\tau = (TL)^{-1} \leq 1/6$, where T is the temperature and L is the Trotter number.

In the following, we fix the band widths as $(D_1, D_2) = (1.0, 2.0)$ and the chemical potential as $\mu = -U/2 - U' + J/4$ to discuss the metal-insulator transitions at half-filling.

III. RESULTS

A. Non-hybridizing bands

Before presenting the results computed at finite temperatures, we briefly summarize the nature of the zero-

temperature phase diagram for $V = 0$ obtained by DMFT together with the exact diagonalization,³ which is shown in Fig. 1. There are three distinct phases depend-

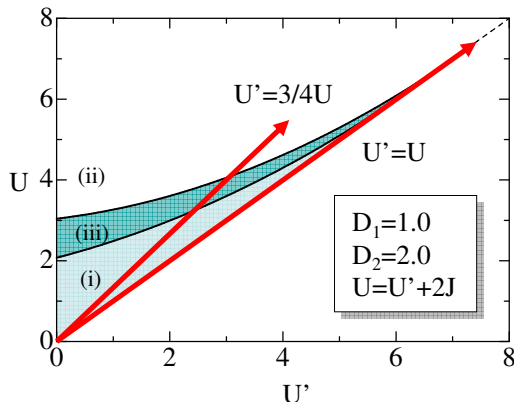


FIG. 1: Phase diagram for the two-orbital Hubbard model with $D_1 = 1$ and $D_2 = 2$. Note that the condition of rotational symmetry, $U = U' + 2J$, is imposed (only the region of $U \geq U'$ is relevant). In the phase (i) (phase (ii)), both bands are metallic (insulating), whereas in the phase (iii) the metallic state coexists with the Mott insulating state. Two lines along $U = U'$ with $J = 0$ and $U'/U = 3/4$ with $J/U = 1/8$ are shown, for which thermodynamic properties at finite temperatures are examined in the text.

ing on the strength of the interactions. It is seen that the metallic phase (i) remains stable up to large Coulomb interaction U along the line $U \sim U'$ (small J), where the Mott transitions merge to a single transition. Away from the symmetric limit, i.e. $U > U'$ with $2J = U - U'$, we find two separate Mott transitions in general. In between the intermediate metallic phase (iii) appears with one band localized and the other itinerant.

We now analyze the temperature dependence of the charge, spin and orbital fluctuations by combining DMFT with QMC simulations. We still restrict here to the case of non-hybridized bands ($V = 0$). Two typical sets of the parameters are considered, which satisfy the conditions $(U'/U, J/U) = (3/4, 1/8)$ and $(1, 0)$. As seen from Fig. 1, the Mott transitions occur at two different critical points $U_{c1} \sim 3$ and $U_{c2} \sim 4$ in the former case, while in the latter case they are merged to a single Mott transition at the critical point $U_c \sim 7$ for zero temperature. The charge (c), spin (s) and orbital (o) susceptibilities are defined as

$$\chi_\gamma = \int_0^\beta d\tau \chi_\gamma(\tau), \quad (8)$$

with $\gamma = c, s, o$, and

$$\begin{aligned} \chi_c(\tau - \tau') &= \langle T | [n(\tau) - 2][n(\tau') - 2] \rangle, \\ \chi_s(\tau - \tau') &= \langle T | [n_\uparrow(\tau) - n_\downarrow(\tau)][n_\uparrow(\tau') - n_\downarrow(\tau')] \rangle, \\ \chi_o(\tau - \tau') &= \langle T | [n_1(\tau) - n_2(\tau)][n_1(\tau') - n_2(\tau')] \rangle, \end{aligned} \quad (9)$$

where T is the time-ordering operator, $n(\tau) = \sum_{\alpha\sigma} n_{\alpha\sigma}(\tau)$, $n_\alpha(\tau) = \sum_\sigma n_{\alpha\sigma}(\tau)$, $n_\sigma(\tau) = \sum_\alpha n_{\alpha\sigma}(\tau)$, and τ is an imaginary time.

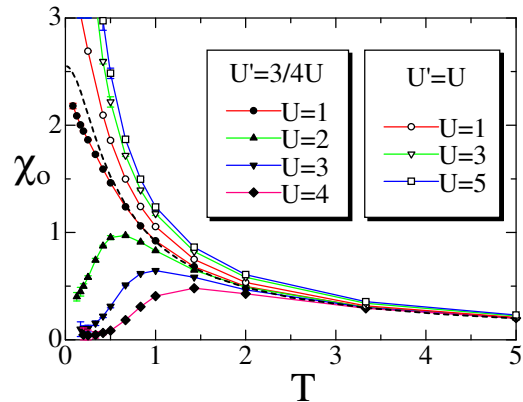


FIG. 2: Orbital susceptibility as a function of the temperature T for $V = 0$. Open (solid) symbols represent the results in the case $U = U'$ and $J = 0$ ($U'/U = 3/4$ and $J/U = 1/8$) and dashed lines those for the non-interacting case.

We first turn to the orbital fluctuations. The temperature-dependent orbital susceptibility is shown in Fig. 2. In the non-interacting system, the orbital susceptibility increases with decreasing temperature, and reaches a constant value at zero temperature. If we now turn on the interactions (fixing the ratios $U'/U = 3/4$ and $J/U = 1/8$), the orbital susceptibility is suppressed at low temperatures. This implies that electrons tend to localized in each band independently such that onsite fluctuations are unfavorable. Eventually for $U \geq U_{c1} \sim 3$, one of the orbitals is entirely localized, so that orbital fluctuations are suppressed completely, giving $\chi_o = 0$ at $T = 0$.

On the other hand, very different behavior can be seen along the line $U' = U$ in Fig. 1. In this case, the orbital susceptibility is increased with growing interactions even at low temperatures. Interpreting this result in the context of the phase diagram in Fig. 1, we can say that the enhanced orbital fluctuations are relevant for stabilizing the metallic phase in the strong correlation regime. While such behavior is naturally expected for models with two equivalent orbitals, it appears even in systems with nonequivalent bands.³⁸

To examine whether the system shows metallic or insulating properties at finite temperatures, we calculate the charge susceptibility (compressibility). The obtained results are shown in Fig. 3. In the case $U'/U = 3/4$ and $J/U = 1/8$, the system with $U = 3$ is located near the critical point between the metallic phase (i) and the intermediate phase (iii). With decreasing temperature the charge susceptibility decreases below $T \sim 1$. The appearance of a pseudogap feature in an intermediate temperature range gives rise to a depletion of density of states at the Fermi energy for both bands. Upon further lowering of the temperature the charge susceptibility

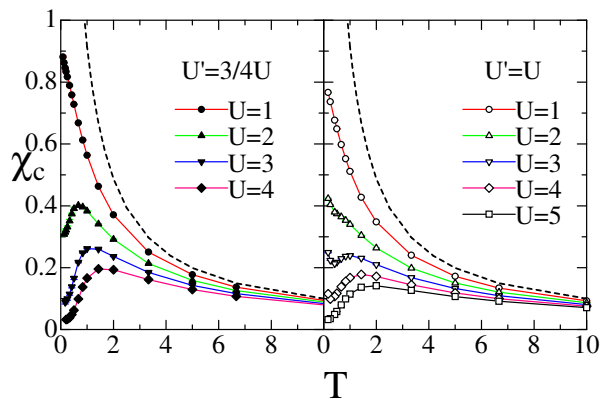


FIG. 3: Charge susceptibility as a function of the temperature T for $V = 0$. Dashed lines represent the results for the non-interacting case.

converges to a finite value, since the system still remains in a metallic phase, at least for one of the two orbitals. For $U = 4$, which corresponds to the boundary between the phases (ii) and (iii), the charge susceptibility at low temperatures is almost zero, suggesting that the system has become completely insulating corresponding to phase (ii). In contrast for $U' = U$ we observe in an intermediate range of U that with lowering temperature a decrease of the charge susceptibility is followed by an eventual increase at lowest temperatures (Fig. 3). Comparing this with Fig. 2, we see that the enhanced orbital fluctuations indeed have a tendency to stabilize the metallic state.

We now move to the spin susceptibility. In Fig. 4,

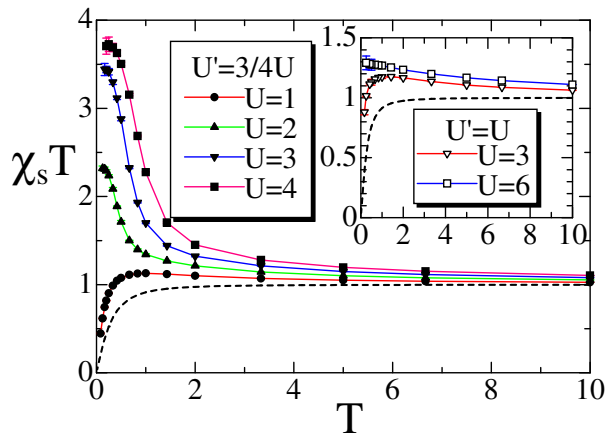


FIG. 4: The effective Curie constant $\chi_s T$ as a function of the temperatures T for $U'/U = 3/4$ and $J/U = 1/8$. Inset shows the results in the case $U' = U$ and $J = 0$. Dashed lines represent the results for the non-interacting case.

we plot the effective Curie constant $\chi_s T$ as a function of the temperature. We first look at the case of $U'/U = 3/4$ and $J/U = 1/8$. At high temperatures, all the spin

configurations are equally populated, so that the effective Curie constant takes the value $1/2$ for each orbital in our units, yielding $\chi_s T \sim 1$. When electron correlations are weak ($U = 1$), the system is still in the metallic phase, so that the Pauli paramagnetic behavior with a constant χ_s emerges, leading to $\chi_s T \rightarrow 0$ as $T \rightarrow 0$. It is seen that the increase of the interactions enhances the spin susceptibility at low temperatures, as a result of the progressive trend to localize the electrons. The effective Curie constant is $\chi_s T = 2$ when a free spin is realized in each orbital. It is seen that the Curie constant increases beyond the value of 2 with the increase of the interactions ($U = 3, 4$). This means that ferromagnetic correlations due to the Hund coupling appear here.

When $U' = U$ (inset of Fig. 4), both spin and orbital fluctuations are enhanced in the presence of the interactions. Accordingly, both spin and orbital susceptibilities increase at low temperatures, forming heavy-fermion states as far as the system stays in the metallic phase (see also Fig. 2). Note that for $U = 6$, at which the system is close to the Mott transition point, the spin susceptibility is enhanced with the effective Curie constant $\chi_s T \sim 4/3$ down to very low temperatures, as seen in the inset of Fig. 4. The value of $4/3$ immediately follows if one takes into account two additional configurations of doubly-occupied orbital besides four magnetic configurations, which are all degenerate at the metal-insulator transition point. Although not clearly observed in the temperature range shown, $\chi_s T$ should vanish at zero temperature for $U = U' = 6$, since the system is still in the metallic phase, as seen from Fig. 1.

To see the above characteristic properties more clearly, we show the density of states for each orbital in Fig. 5, which is computed by the maximum entropy method.^{47,48,49} When the interactions increase along the line $U'/U = 3/4$ and $J/U = 1/8$, the OSMT should occur. Such tendency indeed appears at low temperatures in Fig. 5(a). Although both orbitals stay in metallic states down to low temperatures ($T = 1/6$) for $U = 1$, the OSMT seems to occur for $U = 2$; namely one of the bands develops the Mott Hubbard gap, while the other band still remains metallic. At a first glance, this result is slightly different from the ground-state phase diagram shown in Fig. 1, where the system is in the phase (i) even at $U = 2$. However, this deviation is naturally understood if we take into account the fact that for $U = 2$, the narrower band is already in a highly correlated metallic state, so that the sharp quasi-particle peak immediately disappears as the temperature increases beyond the small characteristic energy scale. This explains the behavior observed in the density of states at $T = 1/6$. For $U = 3$, both bands are insulating at $T = 1/6$ (the system is almost on the boundary between the phases (ii) and (iii) at zero temperature).

In the case $U' = U$, as expected we encounter the qualitatively different behavior shown in Fig. 5. In this case, both bands gradually develop quasi-particle peaks as the interactions increase, and they still remain metallic even

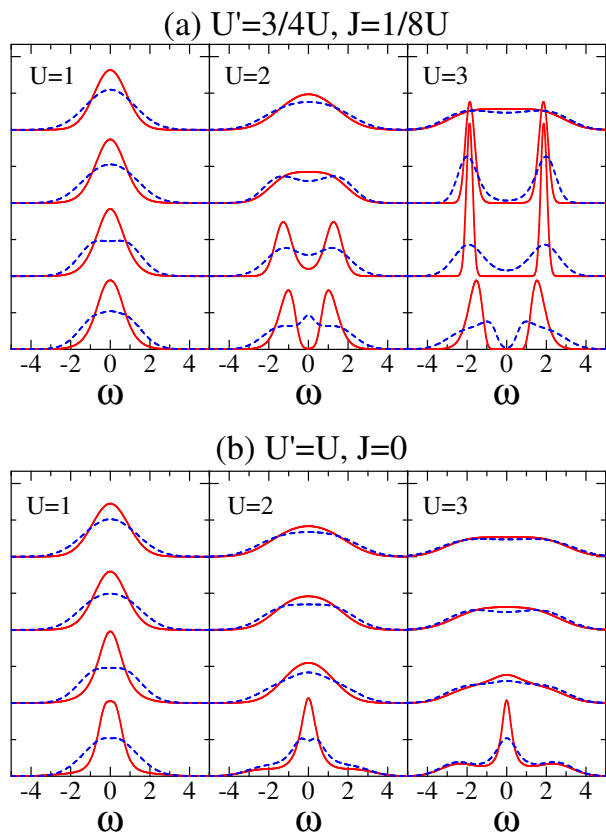


FIG. 5: Density of states for the degenerate Hubbard model $(D_1, D_2) = (1.0, 2.0)$. The data are for the temperatures $T = 2, 1, 1/2$ and $1/6$ from the top to the bottom.

at $U = U' = 3$. As mentioned above, all these features which are in contrast to the situation for $U' \neq U$, are caused by the special symmetry for $U = U'$, which gives rise to equally enhanced spin and orbital fluctuations.

B. Hybridization between distinct orbitals

We have so far treated the degenerate Hubbard model, in which two types of orbitals do not mix with each other. In our treatment with DMFT, the Mott insulating phase (ii) as well as the intermediate phase (iii) may be unstable against certain perturbations. There may be several possible mechanisms that stabilize such insulating phases. One of the mechanisms, which may play an important role in real materials, is the hybridization between the two distinct orbitals. We address the effect in this section.

This hybridization effect is relevant in some real materials. For instance, in the compound $\text{Ca}_{2-x}\text{Sr}_x\text{RuO}_4$,⁷ the hybridization between $\{\alpha, \beta\}$ and γ orbitals is induced by the tilting of RuO_6 octahedra in the region of Ca-doping $0.2 < x < 0.5$,¹¹. This leads to Kondo-lattice like effective model and may be connected with

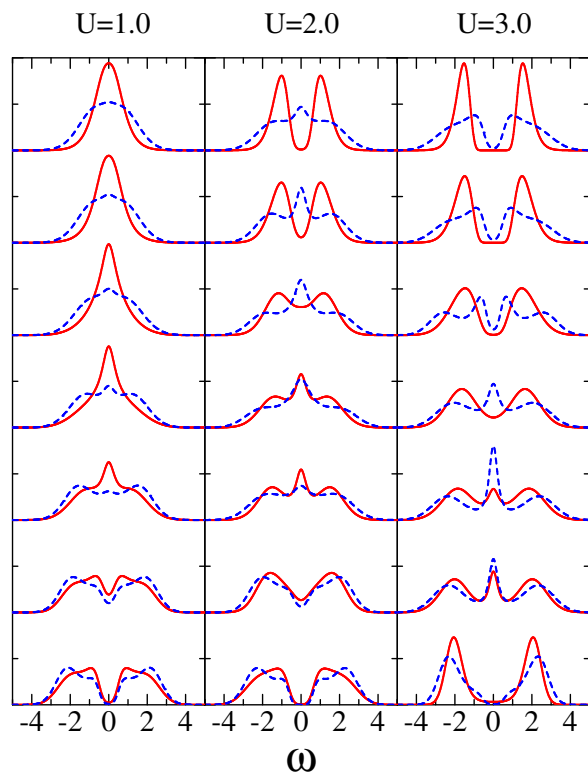


FIG. 6: Solid (dashed) lines represent the density of states for the orbital $\alpha = 1$ ($\alpha = 2$) when $(D_1, D_2) = (1.0, 2.0)$ at $T = 1/6$ with the fixed parameters of $U'/U = 3/4$ and $J/U = 1/8$. The data are plotted for $V = 0.0, 0.25, 0.5, 0.75, 1.0, 1.25$ and 1.5 from top to bottom.

the reported heavy fermion behavior,⁷ similar to some f -electron systems. This interesting aspect motivates us to study the mixing effect between the localized and itinerant electrons in the intermediate phase (iii). Moreover the compound $\text{La}_{n+1}\text{Ni}_n\text{O}_{3n+1}$ ⁸ possesses hybridization between $d_{3z^2-r^2}$ and $d_{x^2-y^2}$ orbitals in the e_g subshell. The OSMT may lead to the metallic but the less-conducting state is realized below the critical temperature $T_c = 550\text{K}$.⁹ Consequently we would like also to explore how the hybridization of different-type d -bands affects electronic properties especially around the OSMT.

We study the general case with $U' \neq U$ and $J \neq 0$ in the presence of the hybridization V . In Fig. 6, the density of states calculated by the maximum entropy method is shown for different choices of V . We start with the weak coupling case, $U = 1$, where the metallic states are realized in both orbitals at $V = 0$. Although the introduction of small V does not alter the nature of the ground state, further increase of V splits the density of states ($V = 1.5$), signaling the formation of the band insulator: namely all kinds of elementary excitations possess the gap. In contrast, we encounter different behavior when electron interactions are increased up to $U = 2$ and 3 . In these parameters, the system at $V = 0$ shows the in-

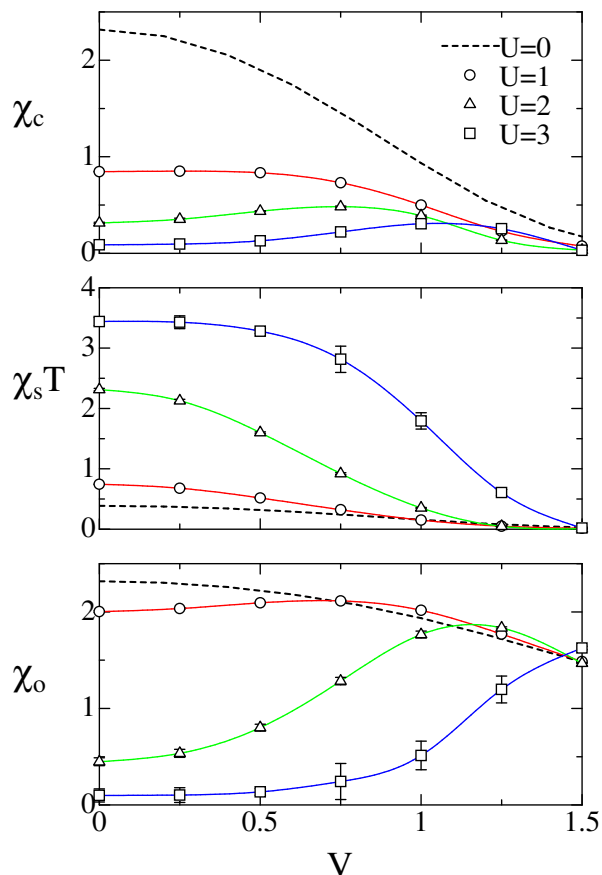


FIG. 7: Charge, spin and orbital susceptibilities as a function of the hybridization V at the temperature $T = 1/6$.

intermediate or Mott-insulating properties at $T = 1/6$. It is seen that the density of states around the Fermi level increases as V increases. For $U = 2$, the intermediate state is first changed to a metallic state, where the quasi-particle peaks appear in both orbitals ($V = 0.75, 1.0$). For fairly large V , both bands fall into the renormalized band insulator ($V = 1.5$). Similarly, for $U = 3$, the hybridization first drives the Mott-insulating state to an intermediate one, as is clearly seen at $V = 0.75$, which is followed by two successive transitions as is the case for $U = 2$.

The above characteristic properties also emerge in the charge, spin and orbital susceptibilities at low temperature, as shown in Fig. 7. For weak interactions ($U = 1$), the charge susceptibility χ_c monotonically decreases with the increase of V . When electron correlations become strong, the non-monotonic behavior appears in χ_c : the charge fluctuations, which are suppressed at $V = 0$, are somewhat recovered by the hybridization, which leads to metallic behavior. For large V , χ_c is again suppressed since the system turns into a band insulator. We can see that the orbital susceptibility exhibits non-monotonic behavior similar to the charge susceptibility, the origin of which is essentially the same as in χ_c ; the orbital fluctu-

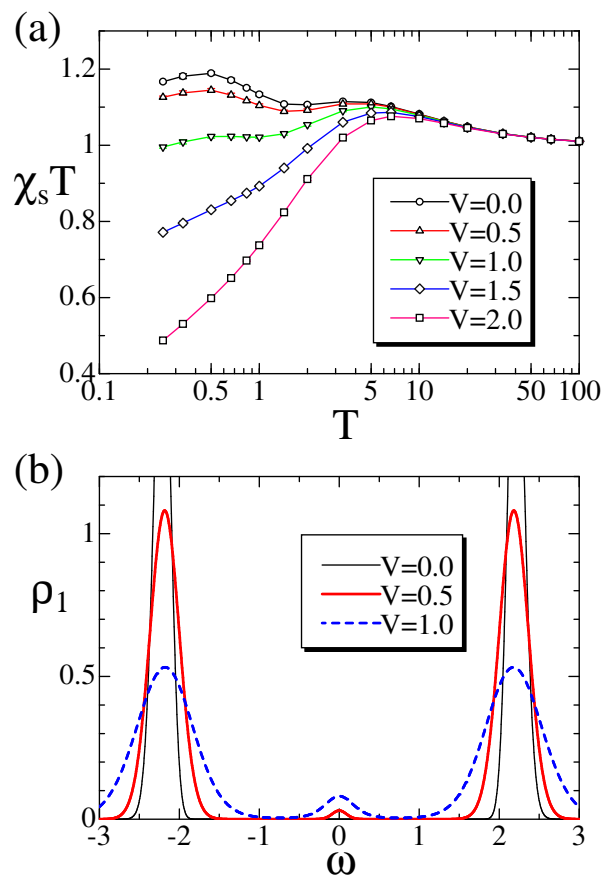


FIG. 8: (a) Effective Curie constant as a function of the temperature and (b) density of states in the narrower band ($\alpha = 1$) at $T = 1/4$ for an extreme choice of the bandwidths, $(D_1, D_2) = (1.0, 10.0)$. The density of states for the wider band is not shown here. The other parameters are $U = 4.0$, $U' = 3.0$ and $J = 0.5$.

ations suppressed at $V = 0$ are recovered by V , and then the formation of the band insulator causes the gradual decrease of χ_o . In contrast, the spin susceptibility monotonically decreases with the increase of V irrespective of the strength of the interactions. As discussed for $V = 0$, the effective spin is enhanced by ferromagnetic fluctuations due to the Hund coupling in the insulating and intermediate phases. Upon introducing the hybridization in these phases, the ferromagnetic fluctuations are suppressed, leading to the monotonic decrease of the effective Curie constant.

From the above observations, we can say that the introduction of appropriate hybridization induces heavy-fermion metallic behavior. In fact, this tendency can be observed more clearly in an extreme choice of the bandwidths, $(D_1, D_2) = (1.0, 10.0)$, shown in Fig. 8. At $V = 0.0$, the system is in the intermediate phase, so that the completely localized states [Fig. 8 (b)] appear in the narrower band in the background of the nearly free bands. This double structure in the system gives rise to

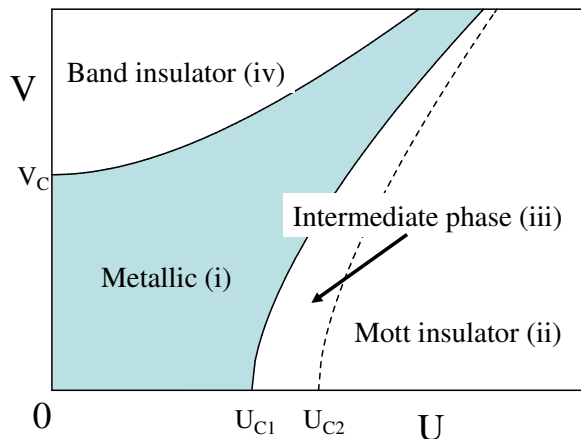


FIG. 9: Schematic phase diagram for the two-orbital Hubbard model with finite hybridization between two orbitals. Solid lines represent the phase boundaries between the metallic and insulating phases. Dashed line indicates the crossover between the Mott insulator and the Kondo insulator.

two peaks in the temperature-dependent effective Curie constant, as shown in Fig. 8 (a). Since the completely localized state plays a role of the f -state in the Anderson lattice model,¹⁰ a "heavy-fermion" peak appears at the Fermi energy in the presence of V , which is essentially the same as that observed in Fig. 6.

Finally, some comments are in order on the phase diagram at zero temperature. In our approach, it is not easy to deal with the system at very low temperatures, since QMC simulations suffer from minus sign problems. Nevertheless, we may give some qualitative arguments on the expected phase diagram at zero temperature. As discussed above, the metallic phase (i) is not so sensitive to V as far as it is small. This is also the case for the completely insulating phase (ii). In contrast, a more subtle situation appears in the intermediate phase (iii). As mentioned above, the intermediate phase exhibits Kondo-like heavy fermion behavior at low temperatures in the presence of V . Recall, however, that we are now concerned with the half-filled band. Therefore, this Kondo-like metallic phase should acquire a Kondo-insulating gap due to commensurability at zero temperature. We would thus say that the intermediate phase (iii) is changed into the Kondo-insulator with a tiny excitation gap in the presence of V at zero temperature. Accordingly, the sharp transition between the phases (ii) and (iii) at $V = 0$ may be smeared and changed to crossover behavior. These considerations lead us to a schematic description of phase diagram for the two-orbital model with mixing between the distinct orbitals, as shown in Fig. 9. On the line of $V = 0$, the OSMT, which may occur in general choices of the parameters, separates the phase at $V = 0$ into three regions. The metallic phase for small U is simply driven to the band-insulator (iv) beyond a certain critical value of hybridization. The intermediate

phase at $V = 0$ is changed to the Kondo-insulator in the presence of any finite V . This insulating state first undergoes a phase transition to the metallic phase, and eventually enters the band-insulator as V increases. The completely Mott insulating phase first shows a crossover to the Kondo insulator, which is further driven to the metallic phase and then to the band-insulating phase. Note that at finite temperatures above the Kondo-insulating gap, we can observe a Kondo-type heavy fermion behavior in the intermediate phase with finite V .

IV. SUMMARY

We have investigated the degenerate Hubbard model with distinct hopping integrals by combining DMFT with QMC simulations. By examining the spin, charge and orbital susceptibilities calculated at finite temperatures, we have clarified that equally enhanced spin and orbital fluctuations play a vital role on stabilizing the metallic states in the multi-orbital systems. This remarkable effect is responsible for whether the system undergoes a single Mott transition or OSMTs. Also, we have discussed how the phase diagram at finite temperatures slightly deviates from the ground-state one because of smearing effect of the narrow quasi-particle peak.

We have further explored the effect of the hybridization between the distinct orbitals, and have found that it plays a crucial role especially around the OSMT. The introduction of the hybridization in the intermediate phase enhances the charge and orbital fluctuations, inducing the metallic phase with a sharp quasi-particle peak. Accordingly, Kondo-like heavy fermion states show up at finite temperatures, which eventually drop in the Kondo insulating phase for our half-filled bands. We have also pointed out that the hybridization effect smears the sharp OSMT at zero temperature, and changes it to a crossover behavior. Nevertheless, we can still observe the OSMT at finite temperatures.

In this paper, we have used QMC as an impurity solver in DMFT, which is not powerful enough to treat properties at very low temperatures. Therefore, it is desirable to exploit a complementary approach to study such low-temperature properties more precisely, although we have arrived at a reasonable phase diagram at zero temperature. Various remaining open problems could not be addressed in the present study. One of the most important issues to explore is magnetism of the system, which has not been seen here, since we have restricted our attention to the paramagnetic phase. This problem is under consideration.

V. ACKNOWLEDGMENTS

We would like to thank K. Ishida, S. Sakai, S. Nakatsuji and Y. Maeno for useful discussions. This work was partly supported by a Grant-in-Aid from the Ministry of

Education, Science, Sports and Culture of Japan, the Swiss National Science Foundation and the Centre of Theoretical Studies at ETH Zürich. A part of compu-

tations was done at the Supercomputer Center at the Institute for Solid State Physics, University of Tokyo and Yukawa Institute Computer Facility.

-
- ¹ V.I. Anisimov, I.A. Nekrasov, D.E. Kondakov, T.M. Rice and M. Sigrist, *Eur. Phys. J. B* **25**, 191 (2002).
- ² Z. Fang and K. Terakura, *Phys. Rev. B* **64**, 020509(R) (2001); Z. Fang, N. Nagaosa and K. Terakura, *Phys. Rev. B* **69**, 045116 (2004).
- ³ A. Koga, N. Kawakami, T.M. Rice, and M. Sigrist, *Phys. Rev. Lett.* **92**, 216402 (2004).
- ⁴ A. Liebsch, *Europhys. Lett.*, **63**, 97 (2003); *Phys. Rev. Lett.*, **91**, 226401 (2003); cond-mat/0405410.
- ⁵ M. Sigrist and M. Troyer, *Eur. J. Phys. B*, **39**, 207 (2004)
- ⁶ A. Koga, N. Kawakami, T.M. Rice, and M. Sigrist, cond-mat/0406457.
- ⁷ S. Nakatsuji et al., *Phys. Rev. Lett.* **90**, 137202 (2003); S. Nakatsuji and Y. Maeno, *Phys. Rev. Lett.* **84**, 2666 (2000).
- ⁸ K. Sreedhar, *et al.*, *J. Solid State Comm.* **110** (1994) 208; Z. Zhang, *et al.*, *J. Solid State Comm.* **108**, 402 (1994); **117** (1995) 236.
- ⁹ Y. Kobayashi, S. Taniguchi, M. Kasai, M. Sato, T. Nishioka, M. Kontani, *J. Phys. Soc. Jpn.* **65**, 3978 (1996).
- ¹⁰ H. Kusunose, S. Yotsushashi, and K. Miyake, *Phys. Rev. B* **62**, 4403 (2000).
- ¹¹ O. Friedt, *et al.*, *Phys. Rev. B* **63**, 174432 (2001).
- ¹² W. Metzner and D. Vollhardt, *Phys. Rev. Lett.* **62**, 324 (1989).
- ¹³ E. Müller-Hartmann, *Z. Phys. B: Condens. Matter* **74**, 507 (1989).
- ¹⁴ A. Georges, G. Kotliar, W. Krauth and M. J. Rozenberg, *Rev. Mod. Phys.* **68**, 13 (1996).
- ¹⁵ T. Pruschke, M. Jarrell, and J.K. Freericks, *Adv. Phys.* **42**, 187 (1995).
- ¹⁶ J. E. Hirsch and R. M. Fye, *Phys. Rev. Lett.* **56**, 2521 (1986).
- ¹⁷ S. Sakai, R. Arita, and H. Aoki, cond-mat/0405503.
- ¹⁸ P. Coleman, *Phys. Rev. B* **28**, 5255 (1983); **29**, 3035 (1984).
- ¹⁹ T.M. Rice and K. Ueda, *Phys. Rev. Lett.* **55**, 995 (1985); *Phys. Rev. B* **34**, 6420 (1986).
- ²⁰ K. Yamada, K. Yosida, and K. Hanzawa, *Prog. Thero, Phys. Suppl.* **108**, 141 (1992).
- ²¹ Y. Kuramoto, *Z. Phys. B* **53**, 37 (1983).
- ²² C. Kim, Y. Kuramoto, and T. Kasuya, *J. Phys. Soc. Jpn.* **59**, 2414 (1990).
- ²³ C. Zener, *Phys. Rev.* **82**, 4031 (1951).
- ²⁴ P. W. Anderson and H. Hasegawa, *Phys. Rev.* **100**, 675 (1955).
- ²⁵ K. Kubo and N. Ohata, *J. Phys. Soc. Jpn.* **33**, 21 (1975).
- ²⁶ N. Furukawa, *J. Phys. Soc. Jpn.* **64**, 2734 (1995).
- ²⁷ M. Caffarel and W. Krauth, *Phys. Rev. Lett.* **72**, 1545 (1994).
- ²⁸ R. Bulla and M. Potthof, *Eur. Phys. J. B* **13**, 257 (2000); M. Potthoff, *Phys. Rev. B* **64**, 165114 (2001).
- ²⁹ Th. Pruschke, D. L. Cox and M. Jarrell: *Phys. Rev. B* **47** (1993) 3553.
- ³⁰ O. Sakai and Y. Kuramoto, *Solid State Comm.* **89**, 307 (1994).
- ³¹ R. Chitra and G. Kotliar, *Phys. Rev. Lett.* **83**, 2386 (1999).
- ³² J. Joo and V. Oudovenko, *Phys. Rev. B* **64**, 193102 (2001).
- ³³ M. S. Laad, L. Craco and E. Müller-Hartmann, *Phys. Rev. B* **64**, 195114 (2001).
- ³⁴ R. Bulla, *Phys. Rev. Lett.* **83**, 136 (1999).
- ³⁵ A. Georges, G. Kotliar and W. Krauth, *Z. Phys. B* **92**, 313 (1993).
- ³⁶ Th. Maier, M. B. Zöfl, Th. Pruschke and J. Keller, *Eur. Phys. J. B* **7**, 377 (1999).
- ³⁷ Y. Ono, R. Bulla and A. C. Hewson, *Eur. Phys. J. B* **19**, 375 (2001); Y. Ohashi and Y. Ono, *J. Phys. Soc. Jpn.* **70**, 2989 (2001).
- ³⁸ A. Koga, Y. Imai and N. Kawakami, *Phys. Rev. B* **66**, 165107 (2002); A. Koga, T. Ohashi, Y. Imai, S. Suga and N. Kawakami, *J. Phys. Soc. Jpn.* **72**, 1306 (2003).
- ³⁹ T. Momoi and K. Kubo, *Phys. Rev. B* **58**, R567 (1998).
- ⁴⁰ G. Kotliar and H. Kajueter, *Phys. Rev. B* **54**, R14221 (1996); M. J. Rozenberg, *Phys. Rev. B* **55**, R4855 (1997); K. Held and D. Vollhardt, *Eur. Phys. J. B* **5**, 473 (1998); J. E. Han, M. Jarrell and D. L. Cox, *Phys. Rev. B* **58**, R4199 (1998); Y. Imai and N. Kawakami, *J. Phys. Soc. Jpn.* **70**, 2365 (2001); V. S. Oudovenko and G. Kotliar, *Phys. Rev. B* **65**, 075102 (2002); Y. Ono, M. Potthoff and R. Bulla, *Phys. Rev. B* **67**, 035119 (2003); Y. Tomio and T. Ogawa, cond-mat/0407314; Th. Pruschke and R. Bulla, cond-mat/0411186.
- ⁴¹ M. Jarrell, H. Akhlaghpour and T. Pruschke, *Phys. Rev. Lett.* **70**, 1670 (1993).
- ⁴² T. Mutou and D. Hirashima, *J. Phys. Soc. Jpn.* **63**, 4475 (1994);
- ⁴³ T. Saso and M. Itoh, *Phys. Rev. B* **53**, 6877 (1996);
- ⁴⁴ R. Sato, T. Ohashi, A. Koga, N. Kawakami, *J. Phys. Soc. Jpn.* **73**, 1864 (2004).
- ⁴⁵ T. Ohashi, A. Koga, S. Suga, and N. Kawakami, *Phys. Rev. B* **70** 245104 (2004).
- ⁴⁶ L. de' Medici, A. Georges, G. Kotliar, and S. Biermann, cond-mat/0502563.
- ⁴⁷ S. F. Gull, in *Maximum Entropy and Bayesian Methods in Science and Engineering*, ed. G. J. Erickson and C. R. Smith (Kluwer Academic, Dordrecht, 1988) p. 53; J. Skilling (Kluwer Academic, Dordrecht, 1989) p. 45; S. F. Gull, *ibid.* p. 53.
- ⁴⁸ R. N. Silver, D. S. Sivia and J. E. Gubernatis, *Phys. Rev. B* **41**, 2380 (1990); J. E. Gubernatis, M. Jarrell, R. N. Silver and D. S. Sivia, *Phys. Rev. B* **44**, 6011 (1991).
- ⁴⁹ W. F. Press, S. A. Teukolsky, W. T. Vetterling and B. R. Flannery, *Numerical Recipes* (Cambridge University Press, Cambridge, 1992) p. 809.